




**Thermal bistability in laser-cooled trapped ions**A. Poindron, J. Pedregosa-Gutierrez , and C. Champenois   
*Aix-Marseille Université, CNRS, PIIM, Marseille 13397, France* (Received 31 January 2023; accepted 20 June 2023; published 13 July 2023)

The nonlinear dynamics of large ion clouds ( $N \geq 256$  ions) trapped in radio-frequency (rf) traps and coupled to laser cooling give rise to a bistable behavior of the temperature. Numerical simulations of the free evolution of a large three-dimensional spherical cloud is used to characterize how the oscillating field amplitude and the ion number control the rf-heating rate and the switching between the two stable states. We show that the heating rate does not significantly depend on the ion number but strongly depends on the oscillating field. This exhibits the major role played by the density of the ensemble. The competition between the radio-frequency heating and the laser cooling is also discussed. They are used to design scenarios to take advantage of the threshold effect to detect and quantify perturbations by an intruder.

DOI: [10.1103/PhysRevA.108.013109](https://doi.org/10.1103/PhysRevA.108.013109)**I. INTRODUCTION**

Ion traps are experimental tools used to manipulate atomic or molecular ions in quantities ranging from a single ion [1] to thousands of ions [2]. Experiments based on large ion clouds remain a very relevant choice for microwave frequency standards [2], high precision spectroscopy of cold molecular ions [3–5], chemical reaction in the cold and diluted limit [6], or quantum optics in the large cooperative regime [7–9]. In these experiments where the cold ion cloud expands in the three directions, the radio-frequency-driven motion (also known as micromotion) is one of the factors limiting resolution and accuracy in spectroscopy because of the induced Doppler shift [10–12]. It is also the source of the radio-frequency (rf) heating, an energy transfer from the rf source to the thermal motion of the ions, mediated by the Coulomb interaction. This rf heating is responsible for fast transitions from a low-temperature state to a high-temperature state, referred as an “explosive onset” in the first studies about chaotic trajectories of few-ion systems [13]. This is the signature of a strong nonlinear dynamics driven by the Coulomb interactions. So far, few molecular dynamics simulations have studied such features like in Ref. [14], where the dynamics of an ion crystal as large as 512 ions in a three-dimensional (3D) Paul trap concludes that ion clouds at 5 mK show rapid heating when the rf electric field amplitude is large enough. This strong dependence with the amplitude of the rf electric field was confirmed in Ref. [15] where periodic boundary conditions were used to study the translationally uniform ion cloud geometry that is a relevant representation for very elongated clouds in 2D linear quadrupole traps. The work detailed in Refs. [16–18] goes beyond the microscopic description and proposes a universal heating formula to capture the dependence on the rf electric field, ion number, and temperature for a spherical cloud in a 3D Paul trap.

Even if most experimental signals rely on the laser-induced fluorescence involved in Doppler laser cooling, few works have combined the study of rf heating in the context of laser cooling [19,20]. As shown in this article, when Doppler

laser cooling is added to this complex system, a bistable behavior can be observed, where the control parameter is the strength of the rf trapping field and the switching parameter is the temperature of the sample. This bistability has a strong impact on experiments involving large samples like shown in the last part of this article. Here, we study this bistability by computing the rf heating of finite-size ion ensembles by means of molecular dynamics simulations, using the data generated during the free evolution of an ion cloud confined in a linear rf trap. Radio-frequency-heating rates are then directly compared to laser-cooling rates to demonstrate the onset of a bistable behavior for the temperature of the sample. Investigating the effect of the ion number  $N$  and the amplitude of the radio-frequency field, we demonstrate that only the latter has a significant effect on the rf-heating rate, pointing to the cloud density as the controlling parameter. These results are then used to build and justify experimental scenarios based on the control of the switch between the two stable states.

**II. MOLECULAR DYNAMICS SIMULATIONS****A. Model**

The ion ensemble is confined in a linear quadrupole rf trap (inner radius  $r_0 = 2.5$  mm) where each diagonal pair of rods, aligned with the  $Oz$  axis, is supplied with time-oscillating voltage (frequency  $\Omega/2\pi = 2$  MHz) with the opposite phase and a common amplitude  $U_{\text{rf}}$  (for more details, see Ref. [20]). The potential generated in the plane perpendicular to the trap axis is

$$\Phi(x, y, t) = \frac{U_{\text{rf}} \cos(\Omega t)}{r_0^2} (x^2 - y^2). \quad (1)$$

A static voltage,  $U_{\text{dc}}$ , is applied to extra electrodes to generate a quadratic potential,  $\Phi(z)$ , along the  $Oz$  axis, characterized by the frequency  $\omega_z/2\pi$  scaling as  $\omega_z/2\pi = 100 \times \sqrt{U_{\text{dc}}}$  kHz for trapped  $\text{Ca}^+$  ions, of mass  $m = 40$  amu and charge

$Q = +q_e = +1.602 \times 10^{-19}$  C. The equations governing the ion dynamics read

$$\ddot{u}_i + \left( -\frac{\omega_z^2}{2} \pm \frac{2QU_{\text{rf}} \cos \Omega t}{mr_0^2} \right) u_i = \frac{Q^2}{4\pi\epsilon_0 m} \sum_{j=1, j \neq i}^N \frac{u_i - u_j}{|\mathbf{r}_i - \mathbf{r}_j|^3}, \quad (2)$$

$$\ddot{z}_i + \omega_z^2 z_i = \frac{Q^2}{4\pi\epsilon_0 m} \sum_{j=1, j \neq i}^N \frac{z_i - z_j}{|\mathbf{r}_i - \mathbf{r}_j|^3}, \quad (3)$$

for an ion  $i$ , where  $u_i$  stands for  $x_i$  or  $y_i$  and  $\mathbf{r}_i = (x_i, y_i, z_i)$ . Those that govern the motion in the radial plane ( $Ox, Oy$ ) can be recast into the standard Mathieu equations [21] by defining the usual  $q_x$  Mathieu parameter giving the dimensionless rf-trapping electric field. We choose positive  $q_x = (4QU_{\text{rf}})/(mr_0^2\Omega^2)$  and the effective Mathieu parameters  $a_x = a_y$  are defined as  $a_x = -2\omega_z^2/\Omega^2$  [22,23].

The equivalent static pseudopotential [24] is defined by the fundamental oscillation frequencies for a single ion in the radial direction  $\omega_r$  and in the axial direction  $\omega_z$ . By changing the strength of the rf trapping field, characterized by the  $q_x$  parameter, two characteristics of the ion clouds are changed. They are the mean density, which scales like  $q_x^2$  [25,26], and the geometrical aspect ratio, which depends on the potential aspect ratio  $\omega_z^2/\omega_r^2$ . To have only one characteristic changing along the simulations, the ratio  $\omega_z^2/\omega_r^2$  is chosen to be equal to 1 for all the tested Mathieu parameters  $q_x$ , which implies a spherical shape to the ion cloud [26]. To achieve this goal, we compute the continuous fraction [21,27] defining the stability parameter  $\beta_x(a_x, q_x) = 2\omega_r/\Omega$  recursively to impose  $\beta_x^2(a_x, q_x) = -2a_x$ .

## B. Temperature

As the rf-driven motion does not contribute to the temperature, it must not be taken into account in its definition [19,28]. To that purpose, the velocity  $\mathbf{v}_i(t)$  of each ion  $i$  is averaged over one radio-frequency period, to smear out the rf-driven oscillation. The temperature  $T$  is dependant on the time-averaged velocities  $\overline{\mathbf{v}_i(t)}$  like

$$\frac{3}{2}k_B T = \frac{1}{2} \frac{m}{N} \sum_{i=1}^N \overline{\mathbf{v}_i(t)^2}, \quad (4)$$

with  $k_B$  being the Boltzmann's constant. Figure 1 shows the time evolution for this temperature for a sample made of 1024 ions, following a thermalization process that takes the sample to 10 mK [20]. After a few milliseconds of free evolution, we observe a sudden increase of the temperature by 2 orders of magnitude. We have checked that the velocity distribution remains in very good agreement with the Maxwell-Boltzmann distribution along this evolution (Fig. 1).

## III. RADIO-FREQUENCY HEATING AND LASER COOLING

### A. Heating rate

To identify the general characteristics of sudden temperature rises, the heating rate  $H = dT/dt$  is calculated based on a

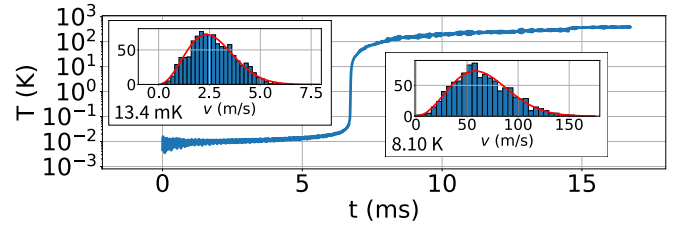


FIG. 1. Temperature evolution of a 1024-ion ensemble, in a trap defined by  $q_x = 0.64$  and  $\omega_z/2\pi = 388$  kHz. The temperature is computed following Eq. (4). The two insets show the velocity distribution of a 1024-ion ensemble at 13.4 mK and 8.10 K as a histogram. The red curve is the computed Maxwell-Boltzmann distribution at this given temperature.

time-averaged temperature to smooth the fluctuations induced by the small size of the sample. The averaging time is chosen as 100  $\mu\text{s}$ , which corresponds to  $n_r = 200$  radio-frequency periods  $\tau_{\text{rf}}$ .

Figure 2 shows these heating rates depending on the temperature computed for a cloud of  $N = 1024$  ions, trapped by five different trapping field amplitudes, characterized by Mathieu parameters  $q_x = \{0.2, 0.3, 0.4, 0.5, 0.6\}$ . Typically, a heating rate curve represented in log-log exhibits the following behavior: at low temperature the heating rate log first increases linearly with the temperature log, going from below  $10^{-6}$  K/ $\tau_{\text{rf}}$  to the range of  $10^{-2}$  K/ $\tau_{\text{rf}}$  for a temperature in the range 0.01–0.1 K. This is the signature of a polynomial dependence of the heating rate on the temperature, with an exponent increasing with  $q_x$ . Then the heating rate remains stationary within the range  $10^{-2}$ – $10^{-1}$  K/ $\tau_{\text{rf}}$  up to 10 K and then it decreases smoothly down to 400 K where simulations are stopped.

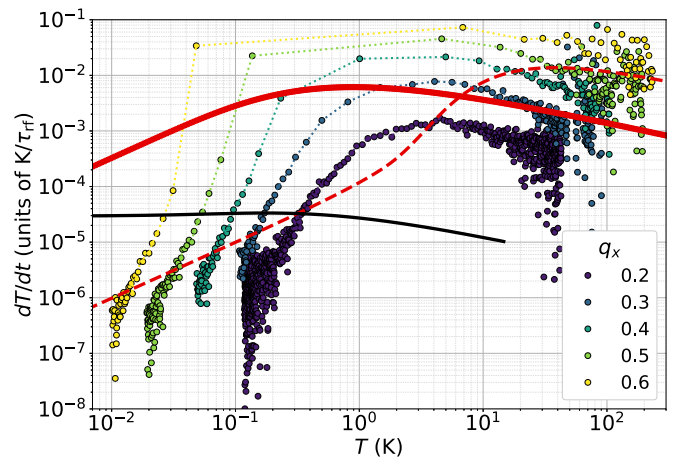


FIG. 2. Log-log representation of  $dT/dt$  vs temperature in a timescale in units of the rf period  $\tau_{\text{rf}}$ . Colored symbols: Free evolution  $H$  of an ensemble of 1024 ions in a rf trapping potential characterized by  $q_x = 0.2, 0.3, 0.4, 0.5$ , and  $0.6$  (see the color chart, the dotted lines are guide to the eyes). Red lines: Cooling rates  $G$  as defined by Eq. (6) for different laser detunings. Solid line:  $\delta_L = -\Gamma$ . Dashed line:  $\delta_L = -10\Gamma$ . Black line: Spontaneous-emission-induced heating  $H_e$  as defined by Eq. (7) for  $\delta_L = -\Gamma$ .

These curves are in accordance with the  $\Lambda$ -shape scheme proposed in Ref. [29] to explain the equilibrium temperature of a trapped ion cloud. For  $q_x = 0.4$ , we find heating rates as a function of temperature in accordance with the results of Ref. [15], computed for  $q_x = 0.44$ . However, we could not confirm that the heating rate behaves universally independently of the Mathieu parameter  $q_x$ , as it was suggested in Ref. [16].

### B. Laser cooling

To characterize the equilibrium thermal state of a laser-cooled sample, we now compare the rf-heating rate to the Doppler laser-cooling rate  $G$ . Doppler laser cooling allows us to cool down ions thanks to the resonant radiation pressure induced by the recoil when ions absorb photons [30,31]. The laser cooling of  $\text{Ca}^+$  ions involves two transitions and three levels but we consider here the simplified model of a two-level system, keeping only the resonant dipole transition at  $\lambda_L = 397$  nm to the first excited state with a lifetime of  $\tau_e = 6.9$  ns [32]. This simplification overestimates the optimum probability  $P_e$  for an ion to be in the excited state by a factor close to 2 [33], but it will not change the conclusion of the comparison. For a laser beam with the wave vector  $\mathbf{k}_L = 2\pi/\lambda_L \mathbf{z}$ , propagating along the symmetry axis  $Oz$  of the trap, the scattering force is [34]  $F_s = \Gamma P_e \hbar \mathbf{k}_L$ , with  $\Gamma = 1/\tau_e$ . The probability  $P_e$  depends on the Rabi frequency  $\Omega_R$  of the laser-dipole coupling, relative to the natural spontaneous emission rate  $\Gamma$ , by the on-resonance saturation parameter  $s = 2\Omega_R^2/\Gamma^2$ . It depends also on the laser frequency  $\omega_L$  by its detuning  $\delta$  from the atomic transition frequency  $\omega_0$  as

$$P_e = \frac{1}{2} \frac{s}{1 + s + 4\delta^2/\Gamma^2}. \quad (5)$$

For a moving atom, the detuning must include the Doppler effect and  $\delta = \delta_L - \mathbf{k}_L \cdot \mathbf{v}$ , with  $\delta_L = \omega_L - \omega_0$ . The work rate (or power) of the radiation pressure force on an ion with velocity  $\mathbf{v}$  can be calculated as  $\mathbf{F}_s \cdot \mathbf{v}$ , assuming that the excitation probability  $P_e$  has reached the stationary limit for a given velocity. This assumption is justified because the transition sets in the broadband limit where  $\Gamma \gg k_L v_r$ , where  $v_r = \hbar k_L/m$  is the recoil velocity due to the absorption of one photon [35]. This work rate, averaged over the ion velocity distribution  $P(\mathbf{v}, T)$  of the sample, defines the cooling rate that we choose to be positive and express in temperature variation per unit of time:

$$G = -\frac{1}{k_B} \int (\mathbf{F}_s \cdot \mathbf{v}) P(\mathbf{v}, T) d\mathbf{v}. \quad (6)$$

For the calculation shown in Fig. 2, a Maxwell-Boltzmann distribution is assumed and the cooling rate is calculated for each temperature, for a saturation parameter of  $s = 2$  and laser detunings of  $\delta_L = -\Gamma$  and  $\delta_L = -10\Gamma$ . To be complete, the comparison of heating and cooling rates must include the heating rate  $H_e$  induced by the spontaneous emission involved in the laser cooling. This can be calculated as [36]

$$H_e = \frac{\hbar^2 k_L^2}{m k_B} \int \Gamma P_e P(\mathbf{v}, T) d\mathbf{v}, \quad (7)$$

in temperature variation per unit of time. The crossing between  $H_e$  and  $G$  gives the low-temperature equilibrium when there is no rf heating. Depending on the chosen laser parameters, it is between 0.5 mK (the Doppler laser limit) and 5 mK.

### C. Competition between rf heating and laser cooling

The comparison between the rf-heating rate  $H$  and the laser-cooling rate  $G$  (see Fig. 2) shows that, except for the smallest value of the Mathieu parameter  $q_x$ , these two curves cross in the low-temperature regime ( $T < 1$  K) as well as in the high-temperature regime ( $T \simeq 100$  K), the rf-heating being dominant between these two borders. We can then define two possible equilibrium temperatures corresponding to  $G = H$ , responsible for the bistable behavior of these systems. For initial conditions such that  $H > G$ , the ensemble converges towards the hotter equilibrium; on the contrary, if  $G > H$ , the cloud converges towards the colder equilibrium. For the low-temperature range the cold-temperature equilibrium is then defined by  $G = H_e$ . For the largest  $q_x$  values, once the low-temperature unstable equilibrium  $G = H$  is crossed,  $H$  reaches its maximum value in a time of the order of magnitude of the averaging window (100  $\mu$ s), which is small with respect to the time elapsed since the beginning of the evolution of the ion cloud at low temperature; hence, this phenomena is usually denoted as an ‘‘explosive onset.’’ For increasing  $q_x$ , the limit temperature for which rf heating dominates laser cooling decreases, from 1 K for  $q_x = 0.3$  to 40 ( $\pm 10$ ) mK for  $q_x = 0.6$ . This illustrates how the trapping parameter  $q_x$  controls the switching conditions between a low-temperature regime and a high-temperature regime.

For the chosen ion number  $N = 1024$  and laser parameters, laser cooling always overcomes rf heating for  $q_x = 0.2$ , except maybe for temperatures of the order of 100 K where the numerical calculations show large fluctuations and are not very relevant. When maximum, the rf-heating rate is 2 to 3 orders of magnitude larger than the spontaneous emission heating rate. It is also the case for larger  $q_x$  values when rf heating overcomes laser cooling. This hierarchy shows that spontaneous emission heating can be neglected when the competition between the two other effects is considered and confirms the role of the  $q_x$  parameter as the controlling figure for rf heating.

The effect of the number of ions on the general trends detailed above is analyzed in Fig. 3 where the rf-heating rate is plotted for  $N = 256, 512$ , and 1024 ions and  $q_x = 0.6$ . It shows that the behavior identified in Fig. 2 is very general for a spherical shape of the ion ensemble as it does not depend significantly on the ion number.

Furthermore, the comparison between  $H$  and  $G$  for this high- $q_x$  regime, as shown in Figs. 2 and 3, shows that in the intermediate-temperature regime where  $H > G$  the rf-heating rate is typically 1 order of magnitude larger than the laser-cooling rate. This justifies under which conditions the impact of laser cooling on the cloud dynamics can be neglected in numerical simulations as well as in experiments.

### D. Effect of the density

For this article,  $q_x$  and  $N$  were varied by factor, respectively, 3 and 4, and the comparison of Figs. 2 and 3 shows

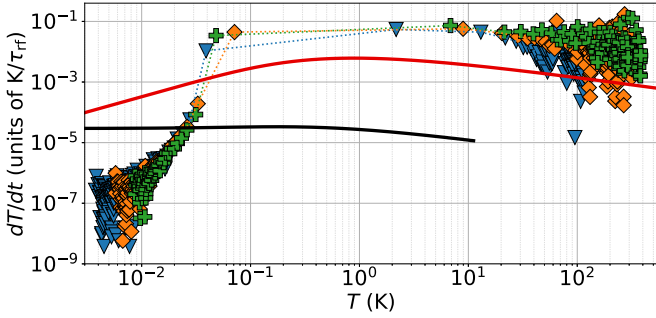


FIG. 3. Log-log representation of  $dT/dt$  vs temperature in a timescale in units of the rf period  $\tau_{\text{rf}}$ . Colored symbols: Free evolution of  $N$  ions and a rf trapping potential characterized by  $q_x = 0.6$ . Blue triangles:  $N = 256$ . Orange diamonds:  $N = 512$ . Green crosses:  $N = 1024$  (the dotted lines are guide to the eyes). Red solid lines: Cooling rate  $G$  as defined by Eq. (6) for the detuning  $\delta_L = -\Gamma$ . Black line: Spontaneous-emission-induced heating  $H_e$  as defined by Eq. (7) for  $\delta_L = -\Gamma$ .

that increasing  $q_x$  has a stronger impact on the rf-heating rate than increasing  $N$ . For  $N = 1024$  ions, the radial size of the ion ensemble decreases from  $R = 190 \mu\text{m}$  for  $q_x = 0.2$  to  $R = 88 \mu\text{m}$  for  $q_x = 0.6$ . For a given trapping condition  $q_x$ , this radial size scales like  $N^{1/3}$  because we chose to keep the cloud spherical. Studying the dependency of the maximum rf electric field reached by the ions as a function of  $q_x$  and  $N$  allows us to show that this field is not the controlling parameter for the heating rate.

Starting from Eq. (1), the electric field amplitude  $\|\mathbf{E}(r)\|$ , controlling the motion of an ion at distance  $r$  to the trap's central axis, scales like  $q_x r$ . In the crystal and liquid phases ( $T \leq 2 \text{ K}$  for the considered densities) [37], the density can be considered as homogenous out of a boundary layer of the order of a few  $\mu\text{m}$  [25,38]. The mean density  $n_c$  scaling with  $q_x^2$  [25,26] and the ion ensemble being spherical,  $NR^{-3} \propto q_x^2$ . Thus, the maximum rf field amplitude for an ion cloud scales like

$$\|\mathbf{E}(R)\| \propto q_x^{1/3} N^{1/3}. \quad (8)$$

Our results demonstrate how  $q_x$  has an effect on the rf-heating rate that is much more significant than that of  $N$ . Nevertheless, Eq. (8) emphasizes how  $q_x$  and  $N$  play a similar role in the maximum electric field reached by the ions. Thus, it is clear that the parameter controlling the rf-heating rate is not  $\|\mathbf{E}(R)\|$ . On the contrary, considering that rf heating is induced by ion-ion collisions, the strong impact of  $q_x$  could be attributed to the change in the mean density which leads to an ion-ion mean distance scaling like  $q_x^{-2/3}$  and is thus reduced by a factor 2.1 by going from  $q_x = 0.2$  to  $q_x = 0.6$ .

#### IV. INSIGHT INTO DIFFERENT EXPERIMENTAL SITUATIONS

In several situations, the collected ion fluorescence is the only nondestructive signal that can be collected from the ion sample, and depending on the laser detuning with the atomic transition, this laser-ion coupling induces Doppler laser cooling [34].

For a constant laser detuning, these systems show a bistable behavior for the temperature, triggered by the Mathieu parameter  $q_x$ , which catches the strength of the rf trapping field. If the  $q_x$  parameter is kept constant, this strong nonlinear behavior shows that a small perturbation in the temperature can be made sufficient to trigger a switch from the low-temperature equilibrium to the high-temperature equilibrium. This perturbation amplification process is at the core of a detection protocol that was proposed to detect giant molecular ions [20,39]. While the temperature increase induced by the energy lost by the projectile  $\Delta E$  is too small to be detected by current laser-induced fluorescence-counting techniques, it can bring the trapped ion cloud to a temperature where the rf-heating rate is orders of magnitude larger, triggering the switch to the high-temperature state. In this thermal state, the Doppler effect results in a reduction of the laser-induced fluorescence rate that is detectable, and the saturation parameter  $s = 2$  and the detuning  $\delta_L = -\Gamma$  were identified as the best compromise for a high sensitivity of the fluorescence signal to the cloud thermal state [20]. In practice, the energy transfer must bring the temperature above the explosive onset threshold where  $G = H$ . This temperature threshold decreases with increasing  $q_x$  and was found to be 20 mK for  $q_x = 0.68$ , 40 mK for  $q_x = 0.6$ , 100 mK for  $q_x = 0.5$ , and 250 mK for  $q_x = 0.4$ . This analysis justifies the need for a large Mathieu parameter for a very sensitive detector, and the temperature thresholds determined according to the method developed in this article are compatible with the previous interaction simulations carried out for  $q_x > 0.5$  [20]. Considering the initial temperature of the ensemble negligible compared to the temperature threshold, the smallest  $q_x$  value for which a detection is observed can produce a measurement of the temperature increase  $\Delta T$  by comparison with numerical data like the one of Fig. 2. As already discussed, the threshold temperature does not depend on the cloud size for typical sizes of hundreds of ions. In a stationary description of the system where we can assume that the ensemble thermalizes after the perturbation by the projectile, we can write  $\Delta E = Nk_B \Delta T$ , and by measuring the number of ions in the cloud [40] the energy lost  $\Delta E$  can be inferred. This control would turn this giant molecular detector into a device able to measure the stopping power of a strongly correlated non-neutral plasma [41,42]. In the small Mathieu parameter regime, the conditions for an intruder to be detected in the observed fluorescence light, assuming no rf heating is amplifying the perturbation, are analyzed in Ref. [43].

Once a detection has been effective, the ion cloud has reached a temperature of the order of 100 K and needs to be cooled down to a temperature lower than the chosen threshold for the next detection, which is lower than 100 mK. For this preparation stage, the bistability analysis are also very useful. As shown in Fig. 2, for a very detuned cooling laser ( $\delta_L = -10\Gamma$ ), the laser-cooling  $G$  overcomes the rf-heating  $H$  for high temperature: above 4 K for  $q_x = 0.2$  and 20 K for  $q_x = 0.4$ . It is then a relevant detuning for cooling ensembles above 100 K, but in order to reach the low-temperature equilibrium, decreasing the detuning alone is insufficient and the Mathieu parameter must be also decreased to reach  $q_x < 0.3$ . With such a low Mathieu parameter, there is always a detuning  $\delta_L$  such that  $G > H$ . It is then possible to bring the

ion ensemble to the low equilibrium temperature by gradually changing the laser detuning from a high  $|\delta_L|$  value to a low  $|\delta_L|$  value. Then,  $q_x$  can be increased to reach the required detection sensitivity, as long as  $G > H$  is verified at the given temperature.

## V. CONCLUSION

This article demonstrates the bistable behavior of a laser-cooled 3D large ion cloud, trapped in a linear rf trap. The comparison between different trapping conditions and cloud sizes allows us to conclude that the characteristic figure controlling the rf-heating rate is the cloud density. This analysis allows us to build a protocol to keep the cold ion cloud in a high trapping field regime and to evaluate the maxi-

imum perturbation that a cloud can absorb without switching to a high-temperature state. Conversely, the possibility to trigger the switch from a low-temperature regime to a high-temperature regime is analyzed in the scope of a detector for giant molecules based on the modification of the cloud fluorescence rate. This detector will take advantage of the amplifying effect induced by the temperature switch, to be sensitive to the crossing of the ion cloud by a single projectile.

## ACKNOWLEDGMENTS

The authors thank David Wilkowski for very stimulating discussions which opened new perspectives for the results presented here. This work is financially supported by CNRS-Innovation (project MegaDalton).

- 
- [1] D. J. Wineland, W. M. Itano, J. C. Bergquist, and R. G. Hulet, *Phys. Rev. A* **36**, 2220 (1987).
  - [2] J. Prestage, R. Tjoelker, G. Dick, and L. Maleki, in *Proceedings of the 45th Annual Symposium on Frequency Control 1991* (IEEE, New York, 1991), p. 572.
  - [3] S. Willitsch, M. T. Bell, A. D. Gingell, and T. P. Softley, *Phys. Chem. Chem. Phys.* **10**, 7200 (2008).
  - [4] S. Alighanbari, M. G. Hansen, V. I. Korobov, and S. Schiller, *Nat. Phys.* **14**, 555 (2018).
  - [5] S. Alighanbari, G. Giri, F. Constantin, V. Korobov, and S. Schiller, *Nature (London)* **581**, 152 (2020).
  - [6] T. Yang, A. Li, G. K. Chen, Q. Yao, A. G. Suits, H. Guo, E. R. Hudson, and W. C. Campbell, *Sci. Adv.* **7**, eabe4080 (2021).
  - [7] A. Dantan, M. Albert, J. P. Marler, P. F. Herskind, and M. Drewsen, *Phys. Rev. A* **80**, 041802(R) (2009).
  - [8] A. Dantan, J. P. Marler, M. Albert, D. Guénot, and M. Drewsen, *Phys. Rev. Lett.* **105**, 103001 (2010).
  - [9] T. Lauprêtre, R. B. Linnet, I. D. Leroux, H. Landa, A. Dantan, and M. Drewsen, *Phys. Rev. A* **99**, 031401(R) (2019).
  - [10] J. Prestage, G. Dick, and L. Maleki, *J. Appl. Phys.* **66**, 1013 (1989).
  - [11] D. Berkeland, J. Miller, J. Bergquist, W. Itano, and D. Wineland, *J. Appl. Phys.* **83**, 5025 (1998).
  - [12] J. Prestage, S. Chung, T. Le, L. Lim, and L. Maleki, in *Proceedings of IEEE International Frequency Control Symposium, Miami, June 5–7, 2006* (IEEE, New York, 2006).
  - [13] J. Hoffnagle, R. G. DeVoe, L. Reyna, and R. G. Brewer, *Phys. Rev. Lett.* **61**, 255 (1988).
  - [14] J. D. Prestage, A. Williams, L. Maleki, M. J. Djomehri, and E. Harabetian, *Phys. Rev. Lett.* **66**, 2964 (1991).
  - [15] V. L. Ryjkov, X. Z. Zhao, and H. A. Schuessler, *Phys. Rev. A* **71**, 033414 (2005).
  - [16] J. D. Tarnas, Y. S. Nam, and R. Blümel, *Phys. Rev. A* **88**, 041401(R) (2013).
  - [17] Y. S. Nam, E. B. Jones, and R. Blümel, *Phys. Rev. A* **90**, 013402 (2014).
  - [18] Y. Nam, D. Weiss, and R. Blümel, *Phys. Lett. A* **381**, 3477 (2017).
  - [19] M. Marciante, C. Champenois, A. Calisti, J. Pedregosa-Gutierrez, and M. Knoop, *Phys. Rev. A* **82**, 033406 (2010).
  - [20] A. Poindron, J. Pedregosa-Gutierrez, C. Jouvét, M. Knoop, and C. Champenois, *J. Chem. Phys.* **154**, 184203 (2021).
  - [21] N. McLachlan, *Theory and Application of Mathieu Functions* (Clarendon, Oxford, 1947).
  - [22] M. Drewsen and A. Brøner, *Phys. Rev. A* **62**, 045401 (2000).
  - [23] A. Drakoudis, M. Söllner, and G. Werth, *Int. J. Mass Spectrom.* **252**, 61 (2006).
  - [24] F. G. Major and H. G. Dehmelt, *Phys. Rev.* **170**, 91 (1968).
  - [25] S. Prasad and T. O’Neil, *Phys. Fluids* **22**, 278 (1979).
  - [26] L. Hornekær and M. Drewsen, *Phys. Rev. A* **66**, 013412 (2002).
  - [27] F. G. Major, V. N. Gheorghe, and G. Werth, in *Charged Particle Traps: Physics and Techniques of Charged Particle Field Confinement*, edited by F. G. Major, V. N. Gheorghe, and G. Werth (Springer, Berlin, 2005), Chap. 2, pp. 17–49.
  - [28] J. P. Schiffer, M. Drewsen, J. S. Hangst, and L. Hornekær, *Proc. Natl. Acad. Sci. USA* **97**, 10697 (2000).
  - [29] R. Blümel, C. Kappler, W. Quint, and H. Walther, *Phys. Rev. A* **40**, 808 (1989).
  - [30] T. Hänsch and A. Schawlow, *Opt. Commun.* **13**, 68 (1975).
  - [31] D. J. Wineland, R. E. Drullinger, and F. L. Walls, *Phys. Rev. Lett.* **40**, 1639 (1978).
  - [32] M. Hettrich, T. Ruster, H. Kaufmann, C. F. Roos, C. T. Schmiegelow, F. Schmidt-Kaler, and U. G. Poschinger, *Phys. Rev. Lett.* **115**, 143003 (2015).
  - [33] C. Lisowski, M. Knoop, C. Champenois, G. Hagel, M. Vedel, and F. Vedel, *Appl. Phys. B* **81**, 5 (2005).
  - [34] H. Metcalf and P. van der Straten, *Laser Cooling and Trapping* (Springer, Berlin, 1999).
  - [35] C. Champenois, *Trapped Charged Particles, Laser Cooling Techniques Applicable to Trapped Ions* (World Scientific, Singapore, 2016), p. 117.
  - [36] P. Lett, W. Phillips, S. Rolston, C. Tanner, R. Watts, and C. I. Westbrook, *J. Opt. Soc. Am. B* **6**, 2084 (1989).
  - [37] J. P. Schiffer, *Phys. Rev. Lett.* **88**, 205003 (2002).
  - [38] C. Champenois, *J. Phys. B* **42**, 154002 (2009).
  - [39] C. Champenois, C. Dedonder-Lardeux, C. Jouvét, L. Hilico, M. Knoop, and J. Pedregosa-Gutierrez, Non-destructive detection method of charged particles without mass limitation, Technical Report, Brevet Européen, 2014.

- [40] M. R. Kamsap, J. Pedregosa-Gutierrez, C. Champenois, D. Guyomarc'h, M. Houssin, and M. Knoop, *Phys. Rev. A* **92**, 043416 (2015).
- [41] G. Zwicknagel, C. Toepffer, and P.-G. Reinhard, *Phys. Rep.* **309**, 117 (1999).
- [42] M. Bussmann, U. Schramm, D. Habs, V. Kolhinen, and J. Szerypo, *Int. J. Mass Spectrom* **251**, 179 (2006).
- [43] M. Gajewski, W. Li, S. Wolf, W. Hahn, C. E. Düllmann, D. Budker, G. Morigi, and F. Schmidt-Kaler, *Phys. Rev. A* **106**, 033108 (2022).